Title
Soft phototactic swimmer based on self-sustained hydrogel oscillator

Journal
Science Robotics, 4(33)

ISSN
2470-9476

Authors
Zhao, Yusen
Xuan, Chen
Qian, Xiaoshi
et al.

Publication Date
2019-08-21

DOI
10.1126/scirobotics.aax7112

Peer reviewed

SOFT ROBOTS

Soft phototactic swimmer based on self-sustained hydrogel oscillator

Yusen Zhao[1], Chen Xuan[2]*, Xiaoshi Qian[1], Yousif Alsaid[1], Mutian Hua[1], Lihua Jin[2], Ximin He[1,3]†

Oscillations are widely found in living organisms to generate propulsion-based locomotion often driven by constant ambient conditions, such as phototactic movements. Such environment-powered and environment-directed locomotions may advance fully autonomous remotely steered robots. However, most man-made oscillations require nonconstant energy input and cannot perform environment-dictated movement. Here, we report a self-sustained soft oscillator that exhibits perpetual and untethered locomotion as a phototactic soft swimming robot, remotely fueled and steered by constant visible light. This particular out-of-equilibrium actuation arises from a self-shadowing–enabled negative feedback loop inherent in the dynamic light–material interactions, promoted by the fast and substantial volume change of the photoresponsive hydrogel. Our analytical model and governing equation unveil the oscillation mechanism and design principle with key parameters identified to tune the dynamics. On this autonomous oscillator platform, we establish a broadly applicable principle for converting a continuous input into a discontinuous output. The modular design can be customized to accommodate various forms of input energy and to generate diverse oscillatory behaviors. The hydrogel oscillator showcases agile life-like omnidirectional motion in the entire three-dimensional space with near-infinite degrees of freedom. The large force generated by the powerful and long-lasting oscillation can sufficiently overcome water damping and effectively self-propel away from a light source. Such a hydrogel oscillator–based all-soft swimming robot, named OsciBot, demonstrated high-speed and controllable phototactic locomotion. This autonomous robot is battery free, deployable, scalable, and integratable. Artificial phototaxis opens broad opportunities in maneuverable marine automated systems, miniaturized transportation, and solar sails.

INTRODUCTION

Phototaxis, spontaneous and directional movement toward or away from light (*1*), has been observed in many living organisms—such as *Platynereis dumerilii* (*2*), jellyfish (*3*), and insects (*4*)—for navigation and photosynthesis. Such stimuli-dictated and environment-powered directional locomotions, if realized with human-made robots, would open new avenues for fully autonomous remotely steered robots. However, artificial phototaxis, the locomotion following illumination direction, has not been realized, despite considerable efforts on photoactuation that have typically been nondirectional (nastic movement) (*5*). Biological phototaxis has typically been realized by helical swimming (*2*) or oscillatory propulsion (*3*). Oscillation is a classic mechanical motion used to generate kinetic energy in propulsion and directional locomotion for various applications, such as robots (*6*), wind-powered drones (*7*), sensing (*8*), and energy coupling (*9*). Current human-made oscillations are typically generated by stimuli variation or intermittent power transmission, such as using AC signals on a piezoelectric transducer. Thus, these systems require a tethered or battery-connected power source and complicated mechanisms. By contrast, living organisms can directly harness energy from a constant ambient environment and produce autonomous oscillations like heartbeats, neuron impulses, circadian clocks, and cell division (*10*). Biological oscillations are mainly out-of-equilibrium phenomena arising from built-in negative feedback loops, which are able to interconvert between two or more kinetically stable states (*10*). If human-made oscillations could be generated using life-like mechanisms and powered by constant environmental sources, it would be extremely advantageous for robotics, especially untethered autonomous robots; however, it remains another great challenge. Hence, the above two challenges in realizing environment-dictated movement directionality and generating oscillatory motion from non-oscillatory ambient input make realizing artificial phototaxis prohibitively difficult.

In recent years, several new materials and mechanisms of oscillation have emerged from attempts to create synthetic active systems that can autonomously oscillate under respective constant stimuli. Examples include chemo-mechanical oscillation based on the Belousov-Zhabotinsky reaction (*11*, *12*) and nonredox reaction (*13*), chemo-mechano-chemical self-regulation (*14*), thermo-mechanical oscillation (*15*), humidity-driven mechanical oscillation (*16*), and pressure-induced mechanical oscillation (*17*). Nevertheless, few of these materials and mechanisms could be applied to create autonomous soft robots, due to constraints on their ability to realize remotely and precisely controlled locomotion of high degrees of freedom (DOFs).

Among several attempts to address these issues, photonic energy has been used because of the synergetic capabilities of wireless signaling, remote powering, and directional control (*18*). Currently, most of the reported work on photoactuation under unsteady state is focused on liquid crystalline networks (LCNs), using preoriented mesogens to induce substantial configuration change associated with the photon-induced phase transition (*19*–*24*). However, limited by the mesogen alignment prerequisite, the LCN-based oscillators are predominantly shaped into thin films, which suffer from single-direction actuation, low available thickness (20 to 50 μm) for generating sufficient forces, complicated fabrication with strict requirements, and limited capabilities to operate with a load or in an ambient environment with a high damping coefficient, i.e., in fluids. Moreover, relying on an anisotropic-isotropic phase transition to power

[1]Department of Materials Science and Engineering, University of California, Los Angeles, Los Angeles, CA 90095, USA. [2]Department of Mechanical and Aerospace Engineering, University of California, Los Angeles, Los Angeles, CA 90095, USA. [3]California Nano-Systems Institute, Los Angeles, CA 90095, USA.
*Present address: Department of Mathematical Sciences, Xi'an Jiaotong-Liverpool University, 111 Ren'ai Rd, 215123, Suzhou, China.
†Corresponding author. Email: ximinhe@ucla.edu

macroscopic motion, the current material systems are quite selective in the input photonic energy, which usually bears high requirements in polarization (*19*–*21*), wavelength (*20*), and narrow operation windows (*25*).

Here, we report a visible light–triggered self-sustained oscillation effect of a hydrogel system showing arbitrary directional motion in fluids with high damping coefficients. The hydrogel oscillator exhibited high scalability (0.36 to 1.1 mm in thickness) and broad operational window (120 to 1125 mW of light) without the need of a polarized light source. Typically, we used a facile one-step synthesis strategy to incorporate the thermally responsive poly(*N*-isopropylacrylamide) (PNIPAAm) hydrogel, which undergoes volumetric change as high as 70% at elevated temperatures (~32°C or other tunable transition temperatures), with gold nanoparticles (AuNPs) embedded as visible light absorbers (fig. S1). To demonstrate the design generality and broad operation condition, we have also achieved hydrogel oscillation under ambient, diffusive light using broadband white light as input and polyaniline (PANi) as absorbers. We achieved oscillatory behavior by establishing a built-in negative feedback loop through self-shadowing and efficient diffusion/mass transfer. The symmetric cylindrical hydrogel pillar design allows for omnidirectional oscillation covering the entire three-dimensional (3D) space at a wide range of deflection angles (the angle between the deflected direction and the initial direction; Fig. 1B) from ±90° to nearly 0° (zenith angles) and 0° to 360° wide azimuthal angles. Through computational analytical modeling, a quantitative model with the governing equation of dynamics was established. It not only has precisely depicted the complex physics and identified the key parameters as a robotic design tool but also enables accurate prediction of oscillation frequency with >90% agreement with the experimental results.

Ultimately, we have demonstrated that this soft agile hydrogel oscillator is capable of producing significant work, specifically propulsion-enabled locomotion. As a soft swimming robot, termed "OsciBot," its efficient self-propulsion mimicked biological negative phototaxis, the behavior of moving away from a light stimulus. This hydrogel oscillator was able to generate remarkably large forces, which were enough to overcome the damping load in an aqueous environment. The OsciBot performed a highly controllable oscillating motion with outstanding output work and hence a fast and controllable swimming speed, >1.15 body lengths/min, which outperforms state-of-the-art soft swimmers. A series of quantitative analyses provided a deeper understanding of the correlation between oscillation parameters and swimming performance. Moreover, the OsciBot could shrink to 5% of its original size in its dry state and reswell in water, making it encapsulatable and deployable on demand. The hydrogel oscillator provides potential in automated systems, soft robotics, miniaturized transport, solar sails, drug delivery, and surgical applications.

RESULTS

For the typical oscillation, an AuNP-embedded PNIPAAm (AuNP/PNIPAAm) hydrogel pillar was mounted vertically on the ground of a water bath, as shown in Fig. 1 (A and B) and movie S1. Upon exposure to a horizontal green laser (532 nm; input power, 175 to 900 mW; beam diameter, 1 mm), the photonic energy was absorbed and converted into thermal energy. With an appropriate pillar diameter, photoabsorber concentration, and light power, the illuminated site of the pillar (referred to as the "hinge" hereafter) reached a local temperature (T) above the lower critical solution temperature (LCST) of PNIPAAm (~32°C), whereas the back side of the hinge remained at a temperature lower than the LCST. The illuminated side with $T >$ LCST therefore shrank as a result of the expulsion of water through diffusing out of hydrogel network, whereas the nonilluminated side remained swollen. Such a photo-triggered asymmetric stretching field induced the pillar to bend toward the light source, followed by continuous and stable oscillation.

The mechanism of self-sustained oscillation is rooted in the photothermally induced self-shadowing effect coupled with the high speed of hydrogel actuation, regulated by a built-in negative feedback loop shown in Fig. 1C. At state 1, an arbitrary spot of the pillar is illuminated and heated above the LCST. The front side of the pillar rapidly shrinks because of fast water diffusion, leading to the overbending (past the equilibrium position determined by the incidence angle) (state 1 – state2) and thus an initial speed caused by inertia. Then, the overbent tip blocks the light source from illuminating the hinge (in the shade), resulting in a decrease of the hinge temperature. At state 2, the tip is at the lowest position with the largest elastic energy, and the temperature is at the LCST, as shown in Fig. 1D. The shadowing by the tip then allows for a continuous cooling of the hinge below the LCST, leading to the rapid reswelling of the gel and pillar unbending (recovery) back to state 3, where the hinge is exposed to light again. Because the hinge temperature is still below LCST and there is an upward velocity, the gel keeps recovering until the temperature reaches the LCST (state 4). At state 4, the tip is at the highest position, also re-storing the largest elastic energy. With the light exposure on the hinge, the temperature keeps increasing to above the LCST, which bends the tip back down to state 1 to start the next cycle. The mechanical oscillation of the tip corresponds to the temperature fluctuation of the hinge (Fig. 1D), exhibiting a 90° phase shift between the two oscillations, which forms a photo-thermo-mechanical negative feedback loop inherent to the light-material interactions. Overall, the mechanism of out-of-equilibrium actuation has two folds: During the dynamic light–material interactions, a self-shadowing–enabled negative feedback loop makes the bending pillar inclined to stay aligned with the light source (equilibrium state photo-tracking, fig. S6A); however, meanwhile, the fast and substantial volume change of the photoresponsive hydrogel generates the (un)bending driving force that is large enough to overcome the water damping, breaking the equilibrium and thus presenting an out-of-equilibrium behavior, oscillatory actuation (fig. S6B).

To identify the material requirements for oscillation to occur, we fabricated hydrogels with a series of cross-linking densities [*N*,*N*′-methylenebis(acrylamide) (BIS) as cross-linker]. The relatively densely cross-linked hydrogel pillars [2.0 weight % (wt %) and 3.0 wt % BIS] reached an equilibrium state, steadily pointing to and tracking the light source, instead of oscillating (fig. S7). By contrast, the loosely cross-linked hydrogel (1.5 wt % BIS) had relatively larger pores (fig. S4), which facilitated fast water diffusion in and out of the hydrogel network, resulting in higher diffusivity (D) and thus rapid volume change (fig. S3). In addition, larger pores also led to a larger degree of volume change than the dense gel under an identical illumination condition (fig. S3). Hence, given the same deflection angle (90°) of the pillar (Fig. 1B), the loosely cross-linked hydrogel deforms a smaller amount across its thickness compared with the relatively dense hydrogels. Smaller deformation depth (t) and the higher diffusivity (D) enable a smaller diffusion time scale (t^2/D) required for reaching a certain deflection angle. This ultrafast deswelling and

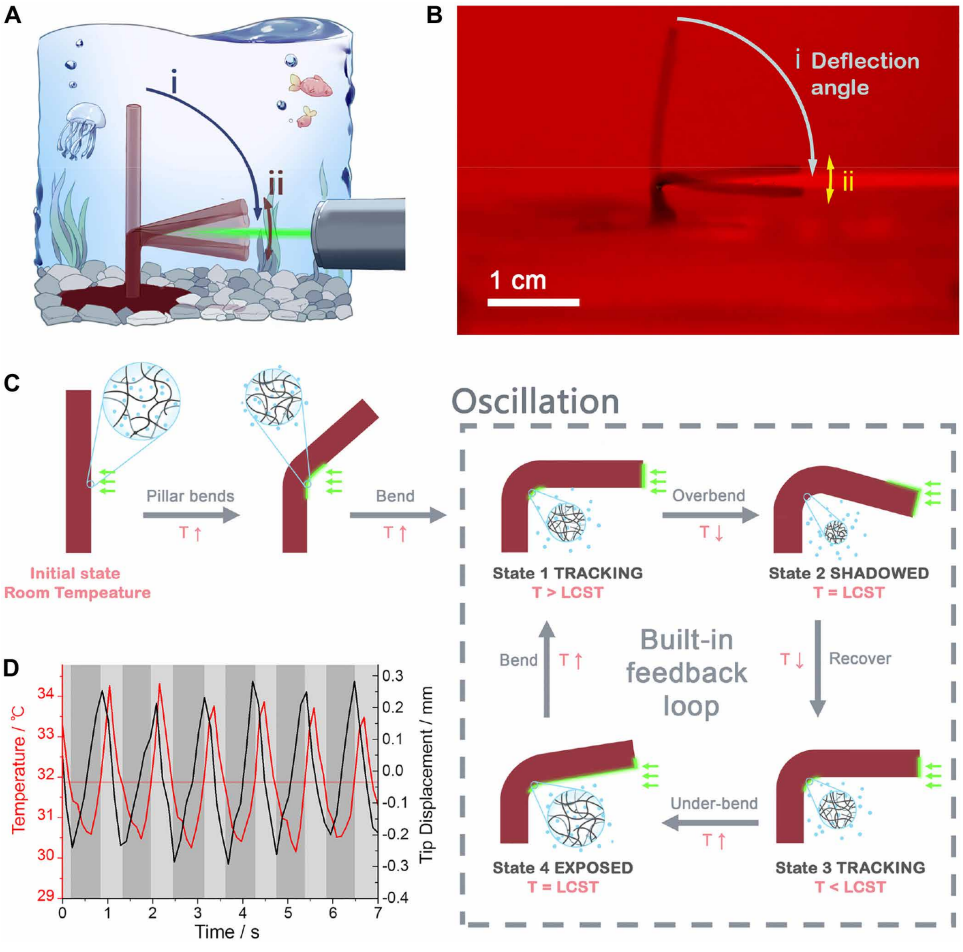

Fig. 1. Light-driven hydrogel oscillator. (**A**) Schematic representation of the gel oscillator and the setup. Initially, the gel-made pillar is placed vertically on the ground in water. As the light is switched on, the gel pillar bends toward the light (step i) and then starts the oscillation (step ii). (**B**) Superimposed frames indicating the tracking followed with oscillation. The gel dimensions are 14 mm (*L*) by 0.9 mm (*d*). (**C**) Mechanism of the oscillation: The out-of-equilibrium actuation is controlled by a self-shadowing–enabled negative feedback loop inherent in the dynamic stimuli-material interactions. Photothermal effect of AuNP induces the temperature increase over the LCST of the PNIPAAm gel, leading to the local shrinkage of the gel and pillar tracking toward the light. Among the oscillation cycles, the tip displacement, temperature, and specific volume of the gel experience periodically change over time. (**D**) Time-resolved tip displacement and local temperature of the hinge for the system with the LCST of 32°C. There is a 90° phase shift of two curves. Dark columns represent the upstroke of the tip, where the temperature is lower than LCST and gel locally recovers. Bright columns, however, represent the downstroke of the tip, where the temperature is higher than LCST and gel locally deswells.

swelling generates large driving forces for deflection and recovery, respectively, which are sufficient to overcome water damping (i.e., the frictional force from the surroundings) and to produce the overshoot of the pillar. This driving force breaks through the equilibrium for the light-tracking state exhibited by the slower-responding gel, facilitates an out-of-equilibrium motion, and also maintains the oscillation (movie S2 and fig. S7).

To further explore the geometrical and spatial requirement of the oscillation, we demonstrated the oscillation of a fishhook pillar (fig. S9A and movie S3), where only the hinge and tip were alternatively exposed to the light. However, the front and back sidewalls of its arm (or cantilever) were not exposed to light and thus did not contribute to the oscillation. The oscillation of fishhook pillar had a similar frequency and amplitude as those of the straight pillar. Also, the oscillation was found to be independent of the original orientation of the pillar, as shown in fig. S9 (B and C) and movie S4 for an example 90° deflection angle. Therefore, the only key requisite for realizing oscillation is rapid and reversible deformation of the exposed hinge, which does not impose constraints on the cantilever geometry or the initial pillar position. Note that the hinge here is not preprogrammed or predesigned in the pillar, which is chemically and structurally homogenous; instead, the hinge is redefinable, because it is instantly formed by the variable light incident on any arbitrary location on the pillar.

To date, most soft actuators and oscillators can achieve only single-directional motion, limiting the DOFs in robotic motion (*19*–*22*). To realize an omnidirectional response to stimuli coming from arbitrary zenith angles (Fig. 2A) and azimuthal angles (Fig. 2B), we designed a chemically homogeneous and geometrically symmetric hydrogel pillar (see movie S5). For an originally upright pillar (d = 0.9 mm), the 500-mW light approached from different oblique angles. We found that an oscillation could be generated with any deflection angle in the range of 59° to 90° (Fig. 2C) with about the same frequency (Fig. 2G). At this particular light power and pillar diameter, an angle smaller than 59° resulted in light tracking (movie S5). To achieve the oscillation at a smaller deflection angle, one approach was to increase the power density of incident light, which increased the driving force as a result. Alternatively, when the pillar diameter was reduced to 0.36 mm, oscillation was realized for deflection angles as small as 8° (Fig. 2D). When the pillar was initially placed horizontally, we realized an oscillation at 0° deflection angle, which has proven hard to achieve in previous reports. Realization of this 0° oscillation perhaps is facilitated by the contribution of the weight of the pillar in the horizontal position in partially providing the driving force downward (Fig. 2E). For this 0° oscillation, by slightly tuning the height of the light with respect to the initially horizontal pillar, a unique asymmetric flapping was achieved (upper-biased flapping and lower-biased flapping, respectively) in addition to the symmetric flapping (fig. S10). Therefore, the wide operation window of deflection angles allows for sophisticated, versatile actuation.

Moreover, we showcased the hydrogel oscillation in response to multiple azimuthal angles (Fig. 2, B and F). Light coming from four different angles covering the entire horizontal plane could all initiate oscillation with the same frequency (Fig. 2H). The oscillation frequency under various zenith angles (Fig. 2G) and azimuthal angles (Fig. 2H) is governed by the frequency formula (Eq. 1) shown below. At this

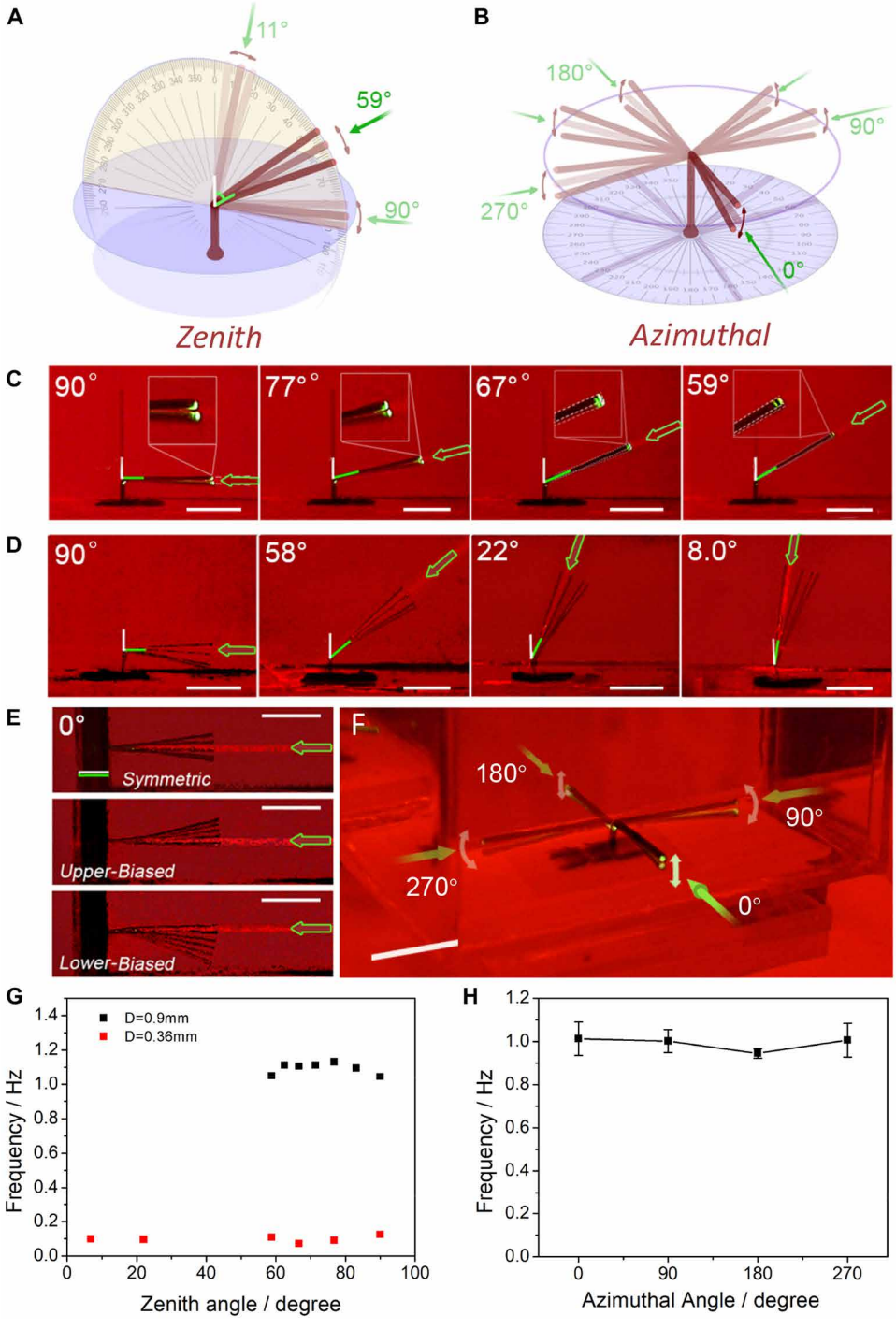

Fig. 2. Realization of omnidirectional oscillation. (**A**) Schematic of zenith scenario, where the pillar is originally placed upright at the bottom with light approaching at different zenith angles. (**B**) Schematic of azimuthal scenario, where the pillar responds to the light approaching at different azimuthal angles. (**C**) Zenith angle test for a pillar with a diameter of 0.9 mm. Under light exposure of 500 mW, the oscillation could be initialized ranging from 90° to 59°. Deflection angle ≤56° resulted in tracking. (**D**) As the diameter was reduced to 0.36 mm, oscillations with 90° to 0° deflection angles and a large oscillation amplitude were observed. Each frame represents 1.3 s for all four different angles. (**E**) Symmetric, upper-biased, and lower-biased oscillations at 0° deflection angle. (**F**) Superimposed snapshots of a pillar in response to different azimuthal angles of light. The frequency dependence of oscillation at (**G**) different zenith angles and (**H**) different azimuthal angles. Error bars indicate SD. (To show the relative positions, all images are superimposed photos of pillars of different configurations at different time points during oscillation.)

stage, we have achieved omnidirectional oscillation at arbitrary zenith and azimuthal angle, exhibiting photo-induced kinetic energy generation in the entire 3D space.

To describe the fundamental physics of the oscillation, we performed analytical modeling to establish a governing equation. First, to characterize the oscillation frequency, we considered the oscillating pillar as a cantilever beam. Because the hydrogel is submerged in water, the damping due to the water cannot be neglected. The angular frequency of the first bending mode of the damped cantilever beam can be calculated as (*26*)

$$\omega_d = \omega_1\sqrt{1-\frac{c^2L^4}{4\rho AEI}} \quad (1)$$

where $\omega_1 \approx 3.5\sqrt{EI/\rho AL^4}$ is the angular frequency of the first bending mode without damping, c is the damping coefficient per unit cantilever length, E is Young's modulus, I is the area moment of inertia, ρ is the hydrogel density, A is the cross-sectional area of the cantilever, and L is the cantilever length (see details in section S5.2). The oscillation frequency ($f_d = \omega_d/2\pi$) for a pillar with a circular cross section of diameter d is then written as (see details in section S5.2)

$$f_d = \frac{3.5}{8\pi}\frac{d}{L^2}\sqrt{\frac{E}{\rho}}\sqrt{1-\frac{64c^2L^4}{\rho E\pi^2 d^6}} \quad (2)$$

According to our experimental data, $E = 6.3$ kPa (see fig. S5), $\rho = 10^3$ kg/m^3, $L \approx 10$ mm, $d \approx 1$ mm, and the natural period of the cantilever vibration without damping is $t_1 = 2\pi/\omega_1 \approx 0.29$ s. Solvent diffusion in the hydrogel has a different time scale of $t_{diff} = d^2/D$, where D is the diffusivity. On the basis of our measurement $D \approx 10^{-7}$ m^2/s, the diffusion time scale t_{diff} can be estimated as around 10 s, which is larger than the inertia time scale. Thus, this model has revealed that the oscillation frequency is dominated by inertia and less influenced by diffusion.

With this model, we further investigated the contributions of inertia and diffusion in the oscillation. Figure 3 and movie S6 illustrate the theoretically and experimentally measured frequency as a function of arm length and diameter. As the arm length increased, the frequency for an undamped cantilever dropped in a scaling of $f_1 = \omega_1/2\pi \approx L^{-2}$, as shown

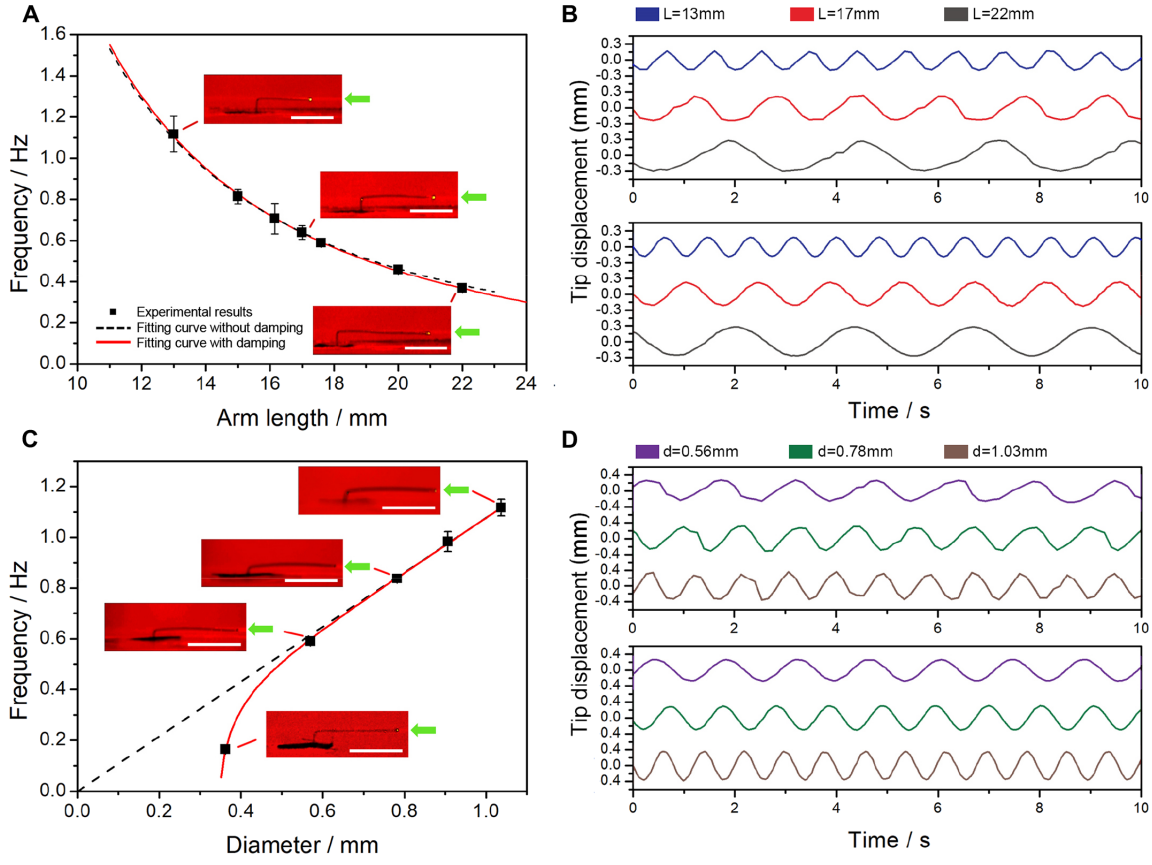

Fig. 3. The frequency of the oscillator dependent on the geometry. (**A**) Frequency as a function of arm length. The fitting curve with water damping consideration matches better with the experimental data (red curve, $R^2 = 0.987$) compared with no water damping (black dashed curve, $R^2 = 0.983$). (**B**) Comparison of the experimental (upper) and computer simulation (lower) result of the time-resolved tip displacement. The dimensions of pillars are as follows: $d = 0.56$ mm; $L = 13$ mm (blue), 17 mm (red), and 22 mm (gray). (**C**) Frequency as a function of diameter. (**D**) Comparison of the experimental and theoretical results. The dimensions of pillars are as follows: $d = 0.56$ mm (purple), 0.78 mm (green), and 1.03 mm (brown); $L = 17$ mm. Input power, 300 mW. Scale bars (in A and C insets), 1 cm. Error bars indicate SD.

by the black dashed curve of Fig. 3A. Considering the water damping of the system, the fitting curve of experimental results will be modified to the red solid curve (see details in section S5.1). To explore the diameter effect, we fabricated pillars with different diameters but the same arm length. The frequency-diameter profile was linear when the diameter was relatively large, consistent with the frequency formula in Eq. 2. However, the water damping term became dominant as the diameter decreased, leading to a deviation from the black line. By fitting the experimental results of the frequency versus diameter plot (Fig. 3C) and the frequency versus arm length plot (Fig. 3A), we obtained the damping coefficients per unit length c to be 3.265×10^{-4} and 1.272×10^{-4}, respectively, which validates the formula of the vibration frequency, Eq. 2 (see details in section S5.1). Furthermore, Fig. 3 (A and C) shows that the experimentally observed oscillation frequency agreed well with the theoretical prediction, verifying the domination of frequency by inertia rather than diffusion. On the other hand, for the pillar to bend to a large angle such as 90°, the water does not need to diffuse through the entire thickness of the hydrogel, but only through a thin layer on the surface. This is sufficient for the hydrogel to bend to a relatively large angle in an oscillation period. Generally, during the oscillation, the diffusivity and speed of bending determines whether there is oscillation or tracking, while the inertia determines the frequency of the oscillation (see details in section S5.4).

In addition, we numerically solved the dynamic oscillation equation for the damped cantilever beam under constant light illumination (section S5.2). The tip displacements for different values of arm length and diameter are shown in Fig. 3 (B and D). The simulated and experimental results for variations in both diameter and arm length show very good agreement, with only ~10% mismatch.

The oscillation performance could also be affected by light intensity. As movie S7 shows, for a hydrogel pillar of certain response rate/ratio and dimension ($L = 17$ mm, $d = 0.36$ to 0.9 mm, 1.5 wt % BIS), an input power lower than a certain threshold (150 to 225 mW) yielded only light tracking. As the input power increased above the threshold, the vibration was amplified cycle by cycle and eventually reached a stable oscillation (fig. S8). A higher light intensity allowed for a broader temperature fluctuation and thus a larger pillar over-bending angle, leading to a higher oscillation amplitude (Fig. 4A). Increasing the input power initially induced a slight frequency drop (Fig. 4B), which may arise from the longer traveling distance required to overcome the water damping and slow down the bending/recovering speed. As the light intensity was increased further, the frequency drop was then compensated by the higher bending speed at a higher light intensity (Fig. 4B). Therefore, the oscillation frequency of the current system solely depends on the geometry and the mechanical properties of the pillar. Moreover, our study indicates that a lower pillar diameter can initiate a higher oscillation amplitude at a given

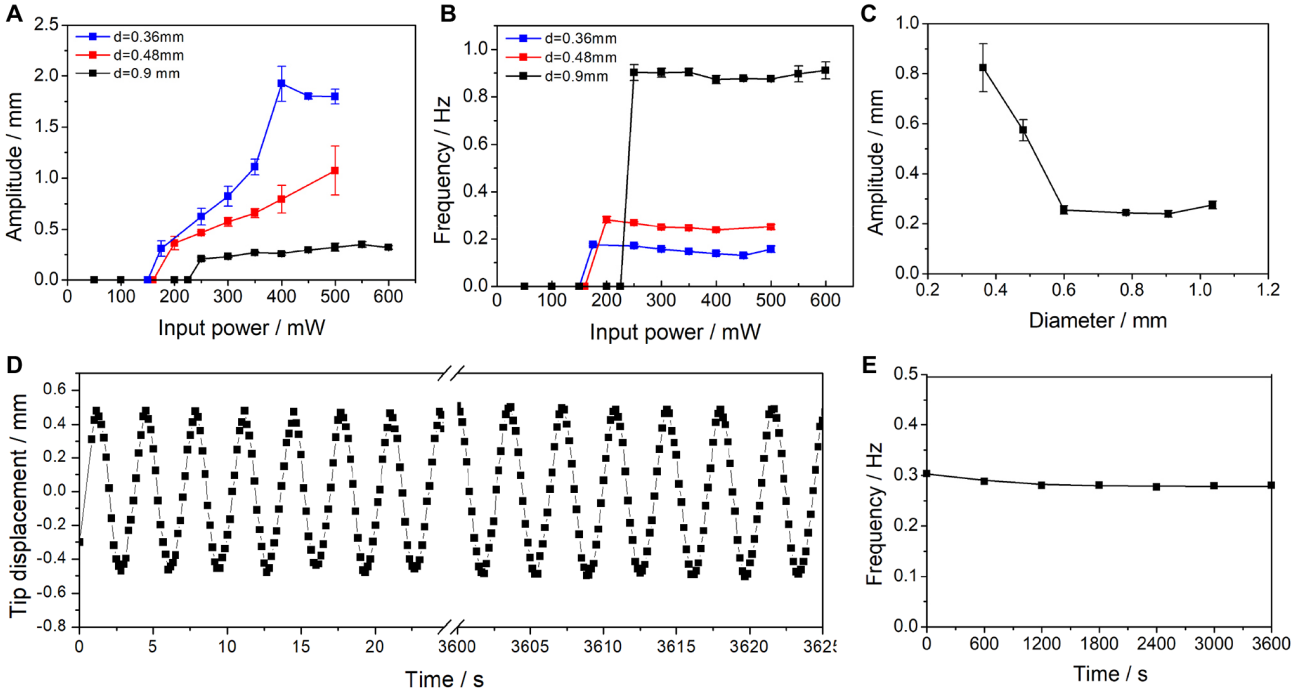

Fig. 4. Input energy dependency and long-term stability of oscillation. (**A** and **B**) Amplitude and frequency as a function of input power. When the input power was higher than the threshold energy, the amplitude increased as input power increased. The frequency, however, maintained a relatively similar value. The thinner pillar could also oscillate with larger amplitude at the same power input. (**C**) Given the same power input of 300 mW, a thinner pillar oscillated at larger amplitude because of a smaller diffusion time scale t^2/D. Tip displacement (**D**) and frequency (**E**) upon irradiation of 200 mW over a long period. The dimensions of the pillar are as follows: $L = 22$ mm and $d = 0.56$ mm. Once reaching steady oscillation, the long-lasting oscillation could be maintained stably over a long period with little frequency and amplitude fluctuation. Error bars indicate SD.

input power (Fig. 4C). The higher amplitude for thinner pillars is due to the smaller t_{diff} for a thin pillar, which results in considerable bending kinetics and magnitudes.

The operation condition of input power was systematically investigated. We summarized the anticipated effects of parameters including the pillar diameter, the arm length, and the absorption (section S4.6). Optimal operation condition of oscillation (blue regime in fig. S11) is defined between the threshold intensity of oscillation (i.e., the minimum input power density required for realizing oscillation) and the unstable intensity, beyond which the oscillation will deviate significantly and be chaotic. First, with a higher arm length, the threshold intensity required to oscillate was gradually reduced, specifically 122 mW for an aspect ratio of 20. In the meantime, the upper limit for stable oscillation (unstable intensity) was also reduced. Second, with a smaller pillar diameter, both the threshold intensity and the unstable intensity were reduced because of the lower t_{diff}. Third, a higher concentration of photoabsorber could also help reduce the threshold intensity and unstable intensity, due to the stronger photothermal effect. Therefore, to reduce the required input power intensity for oscillation, a hydrogel pillar with a larger arm length, a lower diameter, and strong photothermal absorbers would be preferred.

Realizing oscillation using ambient light source is challenging but important for practical applications. On the basis of above analyses of operation condition, we optimized the material composition and geometry to lower the threshold intensity of oscillation to better adapt to the ambient environment with relatively lower light intensity and diffusive direction. Here, we have successfully demonstrated a hydrogel pillar oscillating under broadband white light, which has a spectrum close to that of sunlight and the intensity of 2.5 suns (section S4.7 and movie S11). To respond to this white light, we used PANi as absorbers for its high light absorption efficiency throughout broad wavelength spectra. We also made pillars slightly thinner and longer in arm length (section S2.5) to further lower the threshold intensity. The tip displacement was not as regular as under laser (fig. S12). The oscillation amplitude was slightly chaotic, which might be due to the diffusive light direction making the shadowing less regular. However, the frequency of oscillation stably maintained at ~0.085 Hz, indicating that the oscillation still obeyed the governing equation of frequency.

Figure 4 (D and E) and movie S8 demonstrate the long-term stability of the AuNP-PNIPAAm hydrogel oscillation under prolonged green light exposure. We monitored the motion of the hydrogel oscillator over 3600 s of continuous illumination. It displayed highly stable and relentless long-lasting motion with nearly no noticeable fluctuation. Being continuously fueled by light in a stable environment, the hydrogel pillar is anticipated to oscillate perpetually.

Last, with the powerful oscillator, we successfully created an all-soft phototaxis swimming robot, the OsciBot, capable of propulsion-based high-speed locomotion (Fig. 5A). It is worth pointing out that although there are some propelling robots based on temperature-responsive hydrogels, they mainly rely on the alternating stimuli to achieve the motion (*27*, *28*). However, we can convert the constant energy input into a periodically moving unit in the quest to generate energy-efficient and robust robotic materials. Our swimming robot is made entirely of the same hydrogel material; the design included

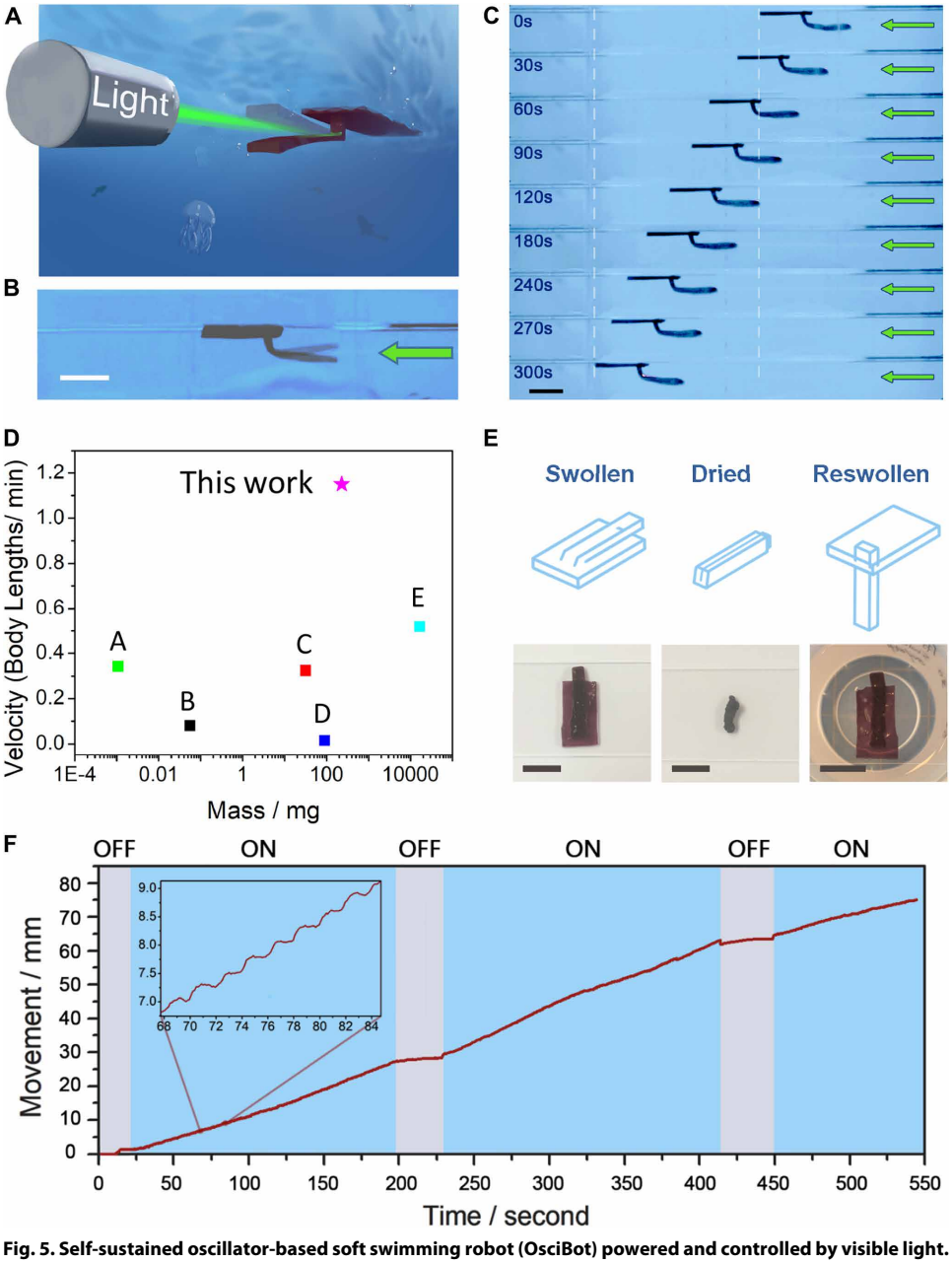

Fig. 5. Self-sustained oscillator-based soft swimming robot (OsciBot) powered and controlled by visible light. (**A**) Scheme of the soft swimmer and (**B**) real oscillation in water. The green arrows denote the light direction. (**C**) Sequential snapshots of swimmer while shining constant light. Input power was 450 mW. (**D**) Velocity versus mass of swimmer in comparison with previous reports. A represents a PDMS-cardiomyocyte biohybrid swimmer (*35*); B represents a ciliate-inspired swimmer (*29*); C represents a flagellum-inspired swimmer (*30*); D represents a hydrogel swimmer under water (*36*); and E represents an eel-inspired microrobot (*37*). (**E**) Comparisons of the fully swollen, thoroughly dried, and reswollen soft swimmer, showing on-demand encapsulating and deployable abilities. Scale bars, 1 cm. (**F**) On/off control of soft swimmer. While the light was switched on, the swimmer kept moving forward. Once the light was switched off, the swimmer stopped in response. During every cycle of the oscillation, mainly the downward stroke (via deswelling) pushed the swimmer forward, resulting in the step-by-step movement over time.

a long hydrogel strip, serving as the paddle, attached perpendicular to a planar hydrogel sheet (fig. S13). As Fig. 5B shows, the robot could float on water because of surface tension on the hydrogel sheet, despite the slightly higher density of hydrogel than that of water. The strip of OsciBot serves as an active flipper to kick water backward and generate propulsion, providing the force to swim away from the light source. When shining light on an arbitrary position of the flipper, it immediately bent upward, followed by continuous oscillating that propelled the OsciBot to move away from light precisely following the illumination direction.

Figure 5C depicts OsciBot's movement fueled and controlled by light. The maximum measured swimming speed was 18.3 mm/min, equivalent to 1.15 body lengths/min, which outperforms previous photoresponsive soft robots inspired by cilia (*29*) and flagella (*30*) with swimming speeds of 0.08 body lengths/min and 0.32 body lengths/min, respectively (Fig. 5D). We have further investigated the robotic performance quantitatively (sections S4.9 and 5.5) and found that the oscillating parameters—including the frequency, the amplitude, and the tip velocity or the thrust—all affect the swimming velocity. From the different oscillation amplitudes of the same OsciBot with a fixed thickness and aspect ratio of the arm, we observed that the OsciBot swam faster with a larger oscillation amplitude in a linear fashion (Fig. 6A), because the strip propelled more water backward during one cycle. The larger amplitude also indicates longer distance for the strip tip to travel, leading to a slight frequency drop, consistent with our experimental observation in Fig. 4B. Thus, the swimming velocity inversely correlates with the oscillation frequency. Furthermore, we established the correlation of swimming velocity of the OsciBot and the velocity of strip tip displacement. With the strip beating faster, the thrust of cantilever was calculated to increase in a quadratic law (section S5.5). Experimentally, such faster beating resulted in higher swimming velocity. Therefore, a larger thrust leads to higher swimming velocity of the OsciBot. By further increasing the light intensity, improving the light absorption efficiency, and rationally optimizing the geometry of the paddle as well as the substrate, the swimming performance can be further enhanced. In addition, potentially, the speed may also be tuned with the fluid properties and flow structure. For instance, a symmetric, reciprocal oscillation is likely to generate directional movement more efficiently in a non-Newtonian fluid of a low Reynolds number, where the net propulsion is caused by the differential apparent fluid viscosity under asymmetric shearing conditions (*31*).

To demonstrate the controllability and flexibility of the light-induced motion, we examined the swimming behavior by intermittently

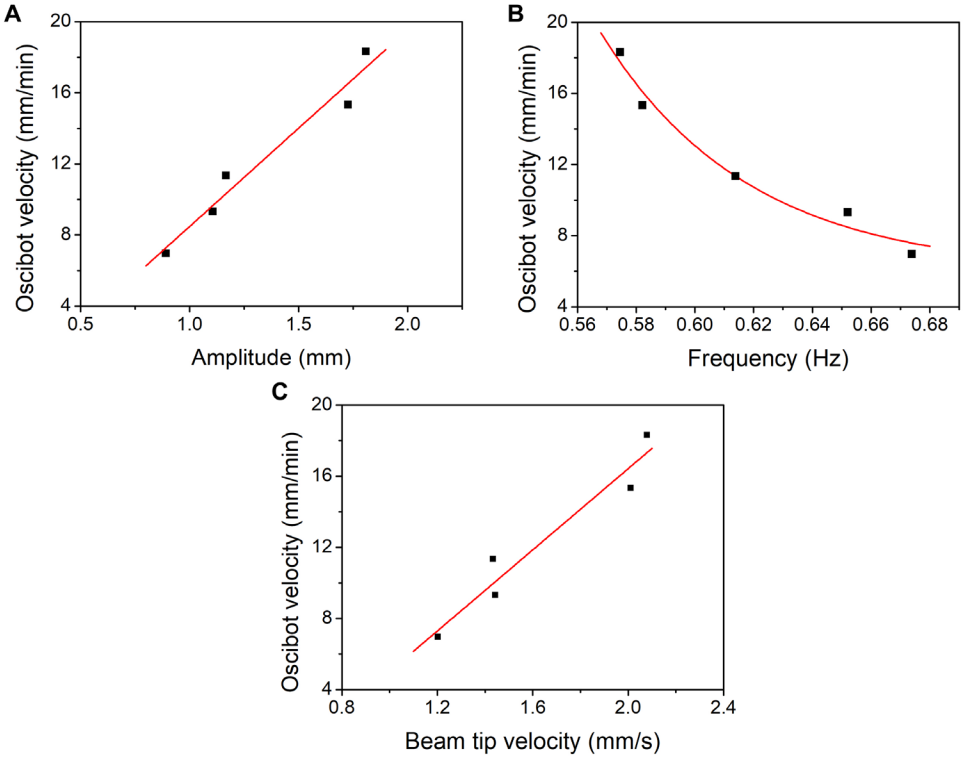

Fig. 6. The effects of oscillation parameters on swimming performance of the OsciBot. OsciBot velocity as the function of (**A**) the amplitude, (**B**) the frequency, and (**C**) the beam tip velocity of the oscillation.

switching the light on and off (Fig. 5F). The swimming robot moved forward at constant speed while the light was on. In the absence of the light, it instantly slowed down and rapidly stopped. Another remarkable point is to determine the dependency of the OsciBot's motion on the upstroke and downstroke during a single cycle. As illustrated by the inset in Fig. 5F, the robot swam forward quickly during every upstroke (deswelling) and moved slowly during every downstroke (recovery and reswelling), exhibiting a stepwise motion. This suggests that the beating-flipper system features a small reciprocating motion effect. With the highly controllable steering directionality, the phototactic locomotion also has demonstrated the potential of maneuverability (section S4.10), owing to the nature of the oscillator precisely following the incident light.

The hydrogel swimmer can also be deployable on demand to perform tasks such as miniaturized packaging and transport. Benefitting from the nature of the hydrogel with a high water content (up to 95.1 ± 0.64% for our system), the soft swimmer could be dried and shrunk to $^{1}/_{20}$th of its original fully swollen size and weight. Thus, as shown in Fig. 5E, the soft swimmer could be encapsulated and stored at a greatly reduced size and then swollen back to its original shape on demand, showing easy portability, good deployability, and robustness.

DISCUSSION

In summary, we have realized artificial phototaxis with an all-soft self-propelled swimmer actuated by the autonomous oscillation of a photosensitive hydrogel under illumination. The phototactic locomotion robot is propelled by autonomous oscillation, which is generated, powered, and controlled by constant visible light. This has advantages from using ambient environmental energy and alleviates an on-board battery or a tether in performing tasks in open water or limited space. With the intelligent material that can perform the lower-level control task using its built-in feedback loop, the overall load on the control system for a robotic system can be significantly reduced, allowing for more sophisticated autonomy and performing previously unachievable complex tasks.

Specifically, we created a conceptually new autonomous oscillator with a constant input. This fundamentally breaks through the conventional pulsed-input-relying oscillation systems. Here, this out-of-equilibrium actuation in particular arises from a self-shadowing–enabled negative feedback loop inherent in the dynamic light–material interactions, promoted by the fast and substantial volume change of the photoresponsive hydrogel. This mechanism is verified by the experimental observation of the periodic tip displacement rhythmically well matched with the time-dependent hydrogel hinge temperature changes. Combining experimental and theoretical modeling, we can expand from this photo-thermal-kinetic self-oscillation generation mechanism into a generic physical principle—how to convert a continuous input into a discontinuous output in different energy forms. One can use the input stimuli–induced responses (e.g., shape or property changes) as the feedback to, in turn, inform and modulate the input. This will form a built-in feedback loop to realize self-control of the material property or environmental condition and to generate periodic behaviors (e.g., mechanical, temperature, or chemical oscillations, such as in local pH or molecular concentration).

Furthermore, this soft oscillator is powerful and robust in generating a force large enough to overcome water damping. This allows it to perform as an all-soft autonomous swimming robot. The OsciBot exhibits negative phototactic movements with a high swimming speed and controllable motion in a high damping environment. The demonstrated phototactic locomotion precisely follows the incident light, showing highly controllable steering directionality and potential maneuverability (section S4.10). This broad-based platform of self-oscillator–based autonomous robots may be expanded from light-driven to be powered by many other input energy forms and switched from aquatic to aerial robots (e.g., flapping-wing flight), with following customizations on material and robotic design.

In terms of materials design, this particular photo-oscillation is achieved by combining photoabsorbers of high photothermal efficiency (fig. S1) with fast and reversible thermally responsive hydrogels. The modular design of responsive materials allows the oscillator platform to be customized and expanded by incorporating a variety of absorbers and stimuli-responsive soft materials that transduce many continuous input stimuli—such as light, pH, (electro)magnetic fields, electric fields, and microwaves—into kinetic energy, in the form of the oscillatory movements and resulting directional locomotion.

In addition, the homogeneous featureless structure of the oscillator makes it convenient to fabricate by additive manufacturing. It may be easily scaled down as a micromachine or scaled up and integrated as an active element into large autonomic systems to meet the requirements for different environments. The untethered, environmental energy–powered robots may perform solar-powered water sampling for oceanographic application.

In terms of robotic motions, the oscillation frequency and amplitude can be tuned by the gel geometry and dimensions and light intensity, as well captured by our established governing equation. With our predictive analytical model, a broad range of oscillatory behaviors may be achieved by tuning or optimizing the oscillator design, oscillation mechanics, and ambient conditions to meet different users' demands (*32*). The self-sustained oscillation provides a versatile capability that may be used in autonomous soft robots, such as submerged swimmers with cilia-like motion (*33*) and transporting devices (*34*). It may also be scaled up or integrated in a large marine vehicle as the active component. Such a self-sustained, tightly controlled, synthetic oscillatory material system may lead to advances in developing robotic counterparts of natural systems. For example, this system may be potentially used for maintaining homeostatic control and generating autonomous oscillations for biomedicine and surgical applications.

MATERIALS AND METHODS

Materials preparation

AuNPs were fabricated using the citrate reduction method (section S2.1). Pillar and swimmer polydimethylsiloxane (PDMS) molds were fabricated by curing PDMS (Sylgard 184) around hypodermic needles of varying gauge widths and 3D-printed swimmer models, respectively, at a 10:1 elastomer–to–curing agent weight ratio at 45°C for 4 hours. The AuNP/PNIPAAm precursor solution was prepared by mixing 40 wt % NIPAAm monomer, 1.5 wt % BIS, 0.5 volume % Darocur 1173, and 0.5 wt % AuNPs in dimethyl sulfoxide (DMSO).

The prepolymer solution was injected into the desired PDMS mold and covered with a 3-(trimethoxysilyl)propyl methacrylate (TMSPMA)–treated cover glass (section S2.3). The hydrogel pillar was cured in its respective PDMS mold under ultraviolet (UV) light for 80 s and then carefully removed and immersed in water to remove DMSO and excess monomer. The OsciBot was fabricated in its respective PDMS mold without the cover glass step and also polymerized under UV light for 80 s.

Characterizations

The tip displacement for all hydrogel was recorded with a digital camera equipped with a red filter. Temperature evolution of the hinge was measured with a thermocouple. The deswelling and swelling kinetics of the hydrogel was measured by heating and cooling a hydrogel cylinder in a water bath. The microstructure was observed with a Supra 40VP scanning electron microscope. The tensile test was measured with the dynamic mechanical analyzer (Q800, TA Instruments). All details of characterization are discussed in the Supplementary Materials.

Simulations

We modeled the hydrogel pillar as a 1D damped cantilever beam. The dynamic vibration equation of the beam with small deflection was formulated. The actuation of the beam is induced by the surface illumination, which causes a temperature gradient and therefore solvent concentration gradient in the thickness direction of the hydrogel. The photo-thermally driven solvent migration was modeled as a 1D diffusion problem in the thickness direction. With the oscillation of the hydrogel, the light spot resides on its top or bottom surface, and the boundary condition of the diffusion equation is switched correspondingly. We solved the coupled diffusion equation and the dynamic vibration equation by the forward-time central-space finite difference method. The parameters that we used in the simulation are laser diameter $d_{ph} = L/20$, cross-link number per monomer volume $N\Omega = 10^{-3}$, polymer-solvent interaction constant $\chi = 0.3$, photochemical potential $\mu_{ph}/k_BT = 5 \times 10^{-4}$, diffusivity $D = 10^{-7}$ m^2/s, density $\rho = 10^3$ kg/m^3, and Young's modulus $E = 6.3$ kPa, unless otherwise stated.

SUPPLEMENTARY MATERIALS

robotics.sciencemag.org/cgi/content/full/4/33/eaax7112/DC1

Materials and Methods
Section S1. General
Section S2. Fabrication of materials
Section S3. Characterization of materials
Section S4. Characterization of oscillation
Section S5. Theory and simulations
Fig. S1. UV-visible absorption spectrum of AuNPs.
Fig. S2. The schematic of the measurement of hydrogel deswelling/swelling ratio and rate.
Fig. S3. Deswelling/swelling kinetics of oscillating hydrogel and tracking hydrogel.
Fig. S4. Scanning electron microscope images of hydrogels.
Fig. S5. The stress-strain curves of hydrogels with different cross-linking densities.
Fig. S6. Photo-tracking versus photo-oscillation.
Fig. S7. Comparisons of the bending and unbending kinetics of oscillating pillar and tracking pillar.
Fig. S8. Switch from tracking to oscillation by tuning light power.
Fig. S9. Fishhook-shaped oscillator and position independency.
Fig. S10. Schematic of lower-biased (case I), upper-biased (case II), and symmetric flapping (case III).
Fig. S11. Range of operation input correlated to the dimension and the photothermal properties.
Fig. S12. Realization of oscillation under ambient white light.
Fig. S13. The hydrogel oscillator floating on the surface of water in the container.
Fig. S14. Maneuverability of the OsciBot.
Table S1. Summary of effect of cross-linking density on materials properties and oscillation performance.
Movie S1. Hydrogel-based light-driven oscillator.
Movie S2. Comparison of light-induced tracking and oscillation.
Movie S3. Fishhook-shaped hydrogel oscillator.
Movie S4. Position independency.
Movie S5. Realization of omnidirectional oscillation.
Movie S6. Oscillation frequency as a function of geometry.
Movie S7. Initialization: From tracking to oscillation.
Movie S8. Long-term stability of the oscillation.
Movie S9. OsciBot: Continuous swimming.
Movie S10. OsciBot: Controllable motion.
Movie S11. Oscillation under ambient white light.
References (*38*–*40*)

REFERENCES AND NOTES

1. E. A. Martin, *Macmillan Dictionary of Life Sciences* (Macmillan Press, ed. 2, 1983).
2. G. Jékely, J. Colombelli, H. Hausen, K. Guy, E. Stelzer, F. Nédélec, D. Arendt, Mechanism of phototaxis in marine zooplankton. *Nature* **456**, 395–399 (2008).
3. T. Katsuk, R. J. Greenspan, Jellyfish nervous systems. *Curr. Biol.* **23**, R592–R594 (2013).
4. E. A. Gorostiza, J. Colomb, B. Brembs, A decision underlies phototaxis in an insect. *Open Biol.* **6**, 160229 (2016).
5. S. Poppinga, C. Zollfrank, O. Prucker, J. Rühe, A. Menges, T. Cheng, T. Speck, Toward a new generation of smart biomimetic actuators for architecture. *Adv. Mater.* **30**, 1703653 (2018).
6. R. Dreyfus, J. Baudry, M. L. Roper, M. Fermigier, H. A. Stone, J. Bibette, Microscopic artificial swimmers. *Nature* **437**, 862–865 (2005).

7. D. Floreano, R. J. Wood, Science, technology and the future of small autonomous drones. *Nature* **521**, 460–466 (2015).
8. P. Puangmali, K. Althoefer, L. D. Seneviratne, D. Murphy, P. Dasgupta, State-of-the-art in force and tactile sensing for minimally invasive surgery. *IEEE Sens. J.* **8**, 371–381 (2008).
9. R. Tang, Z. Liu, D. Xu, J. Liu, L. Yu, H. Yu, Optical pendulum generator based on photomechanical liquid-crystalline actuators. *ACS Appl. Mater. Interfaces* **7**, 8393–8397 (2015).
10. K. Kruse, F. Jülicher, Oscillations in cell biology. *Curr. Opin. Cell Biol.* **17**, 20–26 (2005).
11. R. Yoshida, T. Ueki, Evolution of self-oscillating polymer gels as autonomous polymer systems p. *NPG Asia Mater.* **6**, e107 (2014).
12. S. Maeda, Y. Hara, T. Sakai, R. Yoshida, S. Hashimoto, Self-walking gel. *Adv. Mater.* **19**, 3480–3484 (2007).
13. J. Horváth, Chemomechanical oscillations with a non-redox non-oscillatory reaction. *Chem. Commun.* **53**, 4973–4976 (2017).
14. X. He, M. Aizenberg, O. Kuksenok, L. D. Zarzar, A. Shastri, A. C. Balazs, J. Aizenberg, Synthetic homeostatic materials with chemo-mechano-chemical self-regulation. *Nature* **487**, 214–218 (2012).
15. X.-Q. Wang, C. F. Tan, K. H. Chan, X. Lu, L. Zhu, S.-W. Kim, G. W. Ho, In-built thermo-mechanical cooperative feedback mechanism for self-propelled multimodal locomotion and electricity generation. *Nat. Commun.* **9**, 3438 (2018).
16. B. Shin, J. Ha, M. Lee, K. Park, G. H. Park, T. H. Choi, K.-J. Cho, H.-Y. Kim, Hygrobot: A self-locomotive ratcheted actuator powered by environmental humidity. *Sci. Robot.* **3**, eaar2629 (2018).
17. P. Rothemund, A. Ainla, L. Belding, D. J. Preston, S. Kurihara, Z. Suo, G. M. Whitesides, A soft, bistable valve for autonomous control of soft actuators. *Sci. Robot.* **3**, eaar7986 (2018).
18. H. Koerner, T. J. White, N. V. Tabiryan, T. J. Bunning, R. A. Vaia, Photogenerating work from polymers. *Mater. Today* **11**, 34–42 (2008).
19. T. J. White, N. V. Tabiryan, S. V. Serak, U. A. Hrozhyk, V. P. Tondiglia, H. Koerner, R. A. Vaia, T. J. Bunning, A high frequency photodriven polymer oscillator. *Soft Matter* **4**, 1796–1798 (2008).
20. S. Serak, N. Tabiryan, R. Vergara, T. J. White, R. A. Vaia, T. J. Bunning, Liquid crystalline polymer cantilever oscillators fueled by light. *Soft Matter* **6**, 779–783 (2010).
21. K. M. Lee, M. L. Smith, H. Koerner, N. Tabiryan, R. A. Vaia, T. J. Bunning, T. J. White, Photodriven, flexural–torsional oscillation of glassy azobenzene liquid crystal polymer networks. *Adv. Funct. Mater.* **21**, 2913–2918 (2011).
22. A. H. Gelebart, G. Vantomme, E. W. Meijer, D. J. Broer, Mastering the photothermal effect in liquid crystal networks: A general approach for self-sustained mechanical oscillators. *Adv. Mater.* **29**, 1606712 (2017).
23. A. H. Gelebart, D. J. Mulder, M. Varga, A. Konya, G. Vantomme, E. W. Meijer, R. L. B. Selinger, D. J. Broer, Making waves in a photoactive polymer film. *Nature* **546**, 632–636 (2017).
24. K. Kumar, C. Knie, D. Bléger, M. A. Peletier, H. Friedrich, S. Hecht, D. J. Broer, M. G. Debije, A. P. H. J. Schenning, A chaotic self-oscillating sunlight-driven polymer actuator. *Nat. Commun.* **7**, 11975 (2016).
25. G. Vantomme, A. H. Gelebart, D. J. Broer, E. W. Meijer, Self-sustained actuation from heat dissipation in liquid crystal polymer networks. *J. Polym. Sci. A Polym. Chem.* **56**, 1331–1336 (2018).
26. W. Weaver Jr., S. P. Timoshenko, D. H. Young, *Vibration Problems in Engineering* (John Wiley & Sons, 1990).
27. L. Yeghiazarian, S. Mahajan, C. Montemagno, C. Cohen, U. Wiesner, Directed motion and cargo transport through propagation of polymer-gel volume phase transitions. *Adv. Mater.* **17**, 1869–1873 (2005).
28. F. Vernerey, T. Shen, The mechanics of hydrogel crawlers in confined environment. *J. R. Soc. Interface* **14**, 20170242 (2017).
29. S. Palagi, A. G. Mark, S. Y. Reigh, K. Melde, T. Qiu, H. Zeng, C. Parmeggiani, D. Martella, A. Sanchez-Castillo, N. Kapernaum, F. Giesselmann, D. S. Wiersma, E. Lauga, P. Fischer, Structured light enables biomimetic swimming and versatile locomotion of photoresponsive soft microrobots. *Nat. Mater.* **15**, 647–653 (2016).
30. C. Huang, J.-a. Lv, X. Tian, Y. Wang, Y. Yu, J. Liu, Miniaturized swimming soft robot with complex movement actuated and controlled by remote light signals. *Sci. Rep.* **5**, 17414 (2015).
31. T. Qiu, T.-C. Lee, A. G. Mark, K. I. Morozov, R. Münster, O. Mierka, S. Turek, A. M. Leshansky, P. Fischer, Swimming by reciprocal motion at low Reynolds number. *Nat. Commun.* **5**, 5119 (2014).
32. K. Jain, R. Vedarajan, M. Watanabe, M. Ishikiriyama, N. Matsumi, Tunable LCST behavior of poly (N-isopropylacrylamide/ionic liquid) copolymers. *Polym. Chem.* **6**, 6819–6825 (2015).
33. A. H. Gelebart, M. M. Bride, A. P. H. J. Schenning, C. N. Bowman, D. J. Broer, Photoresponsive fiber array: Toward mimicking the collective motion of cilia for transport applications. *Adv. Funct. Mater.* **26**, 5322–5327 (2016).
34. E. Kizilkan, J. Strueben, A. Staubitz, S. N. Gorb, Bioinspired photocontrollable microstructured transport device. *Sci. Robot.* **2**, eaak9454 (2017).
35. B. J. Williams, S. V. Anand, J. Rajagopalan, M. T. A. Saif, A self-propelled biohybrid swimmer at low Reynolds number. *Nat. Commun.* **5**, 3081 (2014).
36. Y. S. Kim, M. Liu, Y. Ishida, Y. Ebina, M. Osada, T. Sasaki, T. Hikima, M. Takata, T. Aida, Thermoresponsive actuation enabled by permittivity switching in an electrostatically anisotropic hydrogel. *Nat. Mater.* **14**, 1002–1007 (2015).
37. C. Christianson, N. N. Goldberg, D. D. Deheyn, S. Cai, M. T. Tolley, Translucent soft robots driven by frameless fluid electrode dielectric elastomer actuators. *Sci. Robot.* **3**, eaat1893 (2018).
38. G. K. Batchelor, Slender-body theory for particles of arbitrary cross-section in Stokes flow. *J. Fluid Mech.* **44**, 419–440 (1970).
39. D. Tan, P. Yavarow, A. Erturk, Resonant nonlinearities of macro-fiber composite cantilevers in energy harvesting, in *ASME 2017 Conference on Smart Materials, Adaptive Structures and Intelligent Systems* (ASME, 2017), p. V001T07A013.
40. M. J. Lighthill, Note on the swimming of slender fish. *J. Fluid Mech.* **9**, 305–317 (1960).

Acknowledgments: We thank Y. Qiu for help with dynamic mechanical analysis testing for the mechanical properties of the hydrogel. **Funding:** The research was supported by ONR awards N000141712117 and N00014-18-1-2314, AFOSR awards FA9550-17-1-0311 and FA9550-18-1-0449, the Hellman Fellows Funds, and the start-up funds from the University of California, Los Angeles. **Author contributions:** X.H. conceived the concept, planned the project, and supervised the research. X.H. and Y.Z. designed and conducted the experiments and data analysis. Y.Z. and Y.A. conducted the fabrication and characterization. C.X. and L.J. developed the model and numerical code for the analytic modeling. Y.Z., X.H., L.J., M.H., Y.A., C.X., and X.Q. wrote the manuscript. **Competing interests:** Y.Z. and X.H. are inventors on a provisional patent application on the photo-oscillation technology. The other authors declare that they have no competing interests. **Data and materials availability:** All data needed to evaluate and support the conclusions in the manuscript are included in the main text or the Supplementary Materials. Contact Y.Z. for any questions.

Submitted 16 April 2019
Accepted 29 July 2019
Published 21 August 2019
10.1126/scirobotics.aax7112

Citation: Y. Zhao, C. Xuan, X. Qian, Y. Alsaid, M. Hua, L. Jin, X. He, Soft phototactic swimmer based on self-sustained hydrogel oscillator. *Sci. Robot.* **4**, eaax7112 (2019).

Science Robotics

Soft phototactic swimmer based on self-sustained hydrogel oscillator

Yusen Zhao, Chen Xuan, Xiaoshi Qian, Yousif Alsaid, Mutian Hua, Lihua Jin and Ximin He

Sci. Robotics **4**, eaax7112.
DOI: 10.1126/scirobotics.aax7112